
H. Kazerooni
Andrew Chu
Ryan Steger

Human Engineering & Robotics Laboratory
University of California
Berkeley, CA 94720, USA
exo@berkeley.edu

That Which Does Not Stabilize, Will Only Make Us Stronger

Abstract

Many places in the world are too rugged or enclosed for vehicles to access. Even today, material transport to such areas is limited to manual labor and beasts of burden. Modern advancements in wearable robotics may make those methods obsolete. Lower extremity exoskeletons seek to supplement the intelligence and sensory systems of a human with the significant strength and endurance of a pair of wearable robotic legs that support a payload. This article first outlines the use of Clinical Gait Analysis data as the framework for the design of such a system at UC Berkeley. This data is used to design the exoskeleton degrees of freedom and size its actuators. It will then give an overview of one of the control schemes implemented on the BLEEX. The control algorithm described here increases the system closed loop sensitivity to its wearer's forces and torques without any measurement from the wearer (such as force, position, or electromyogram signal). The control algorithm uses the inverse dynamics of the exoskeleton, scaled by a number smaller than unity, as a positive feedback controller. This controller almost destabilizes the system since it leads to an overall loop gain slightly smaller than unity and results in a large sensitivity to all wearer's forces and torques thereby allowing the exoskeleton to shadow its wearer.

KEY WORDS—BLEEX, legged locomotion, lower extremity exoskeleton, biomimetic, clinical gait analysis

1. Introduction

Material transport has been dominated by wheeled vehicles, but many environments such as stairs are simply too treacherous for them to negotiate. Many attempts have been made to develop legged robots capable of navigating such terrain (Raibert 1986). Unfortunately, difficult terrain taxes not only the kinematical capabilities of such systems, but also the sensory, path planning, and balancing abilities of even the most

state-of-the-art robots. Lower extremity exoskeletons seek to circumvent the limitations on autonomous legged robots by adding a human operator to the system. These systems augment human strength and endurance during locomotion. The first load-carrying, field-operational and energetically autonomous lower extremity exoskeleton was designed and built at Berkeley and is commonly referred to as BLEEX. It consists of two powered anthropomorphic legs, a power unit, and a backpack-like frame on which heavy loads can be mounted. This system allows its wearer to carry significant loads with minimal effort. Because the pilot can do this for extended periods of time without reducing his/her agility, the BLEEX increases the physical effectiveness of the pilot. In this initial model, BLEEX offers a payload capacity of 75 lbs (34 kg), with any excess payload being supported by the pilot. The BLEEX lets soldiers, disaster relief workers, firefighters, and other emergency personnel carry major loads without the strain associated with demanding labor. It is our vision that the BLEEX will provide a versatile *load transport platform* for mission-critical equipment.

2. Prior Research Work

Although autonomous robotic systems perform remarkably in structured environments like factories, integrated human-robotic systems are superior in unstructured environments that demand significant adaptation. In our research work at Berkeley, the problems of upper- and lower-extremity human power augmentation were tackled separately. The reasons for this were two-fold; first, there are many immediate applications for stand-alone lower- and upper-extremity exoskeletons. Second, exoskeleton research is still in its early stages, and further research is required before integration of upper- and lower-extremity exoskeletons can be attempted.

In the mid-1980s, we initiated several research projects on upper extremity exoskeleton systems, billed as “human extenders.” The main function of these was human power augmentation for manipulation of heavy and bulky objects (Kazerooni

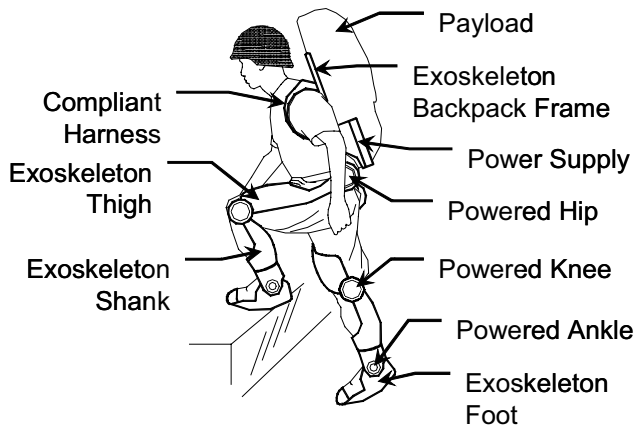


Fig. 1. Initial lower extremity exoskeleton concept at Berkeley. The architecture mimics its human wearer with connections at the wearer's feet and back only. By appropriately actuating joints, the lower extremity exoskeleton supports the payload and removes the weight from the wearer while allowing the wearer to control the balance and motion of the device.

1990, 1996; Kazerooni and Guo 1993). When a worker uses an upper extremity exoskeleton to move a load, the device bears the bulk of the weight while transferring a scaled-down load to the user. In this fashion, the worker can still sense the load's weight and judge his/her movements accordingly, but the force he/she feels is greatly reduced. Since upper extremity exoskeletons are mostly used for factory floors, warehouses, and distribution centers, they are hung from overhead cranes. Lower extremity exoskeletons focus on supporting and carrying heavy payloads on the operator's back (like a backpack) during long distance locomotion.

In the early 1960s, the Defense Department expressed interest in the development of a man-amplifier, a "powered suit of armor" which would augment soldiers' lifting and carrying capabilities. In 1962, the Air Force had the Cornell Aeronautical Laboratory study the feasibility of using a master-slave robotic system as a man-amplifier. In later work, Cornell determined that an exoskeleton, an external structure in the shape of the human body which has far fewer degrees of freedom than a human, could accomplish most desired tasks (Mizen 1965). From 1960 to 1971, General Electric developed and tested a prototype man-amplifier, a master-slave system called the Hardiman (GEC 1968, 1969; Groshaw 1969; Makinson 1971; Mosher 1970). The Hardiman was a set of overlapping exoskeletons worn by a human operator. The outer exoskeleton (the slave) followed the motions of the inner exoskeleton (the master), which followed the motions of the human operator. All these studies found that duplicating all human motions and using master-slave systems were

not practical. Additionally, difficulties in human sensing and system complexity kept it from walking.

Several exoskeletons were developed at the University of Belgrade in the 1960s and 1970s to aid paraplegics (Vukobratovic et al. 1972; Hristic and Vukobratovic 1973). Although these early devices were limited to predefined motions and had limited success, balancing algorithms developed for them are still used in many bipedal robots (Hirai et al. 1998). The "RoboKnee" is a powered knee brace that functions in parallel to the wearer's knee and transfers load to the wearer's ankle (not to the ground) (Pratt et al. 2004). "HAL" is an orthosis, connected to thighs and shanks, that moves a patient's legs as a function of the EMG signals measured from the wearer (Kawamoto and Sankai 2002; Kawamoto et al. 2003).

The Berkeley Lower Extremity Exoskeleton (BLEEX) is not an orthosis or a brace; unlike the above systems it is designed to carry a heavy load by transferring the load weight to the ground (not to the wearer). BLEEX has four new features. First, novel control architecture was developed that controls the exoskeleton through measurements of the exoskeleton itself (Kazerooni and Steger 2006). This eliminated problematic human induced instability (Kazerooni and Guo 1993) due to sensing the human force. Second, a series of high specific power and specific energy power supplies were developed that were small enough to make BLEEX a true field-operational system (Raade and Kazerooni 2004). In particular a fuel based power supply was designed and built that generated electric and hydraulic power simultaneously (Amundson et al. 2005). Third, a body LAN (Local Area Network) with a special communication protocol and hardware were developed to simplify and reduce the cabling task of all the sensors and actuators needed for exoskeleton control (Kim et al. 2004; Kim and Kazerooni 2004). Finally, a flexible and versatile architecture was chosen to decrease complexity and power consumption. This paper describes the biomimetic design of BLEEX and its control algorithm.

3. Exoskeleton Architecture

An anthropomorphic architecture with similar kinematics to a human was chosen for BLEEX. Thus, the exoskeleton has ankle, knee, and hip joints similar to human legs. BLEEX rigidly attaches to the operator at the feet via custom boots and bindings and at the torso through a custom vest. Other connections between pilot and device were allowed, but only if they were compliant so that load does not transfer to the pilot. The exoskeleton legs can therefore follow the human's, but are not required to match exactly since there are only two rigid attachments between human and exoskeleton. The connection at the torso is made using a custom vest which allows the distribution of the forces between BLEEX and the pilot, thereby preventing abrasion. These vests are made of several hard surfaces that are compliantly connected to each other us-

ing thick fabric. The vests include rigid plates on their backs for connection to the BLEEX spine. Each BLEEX leg has three degrees of freedom at the hip, one degree of freedom at the knee, and three degrees of freedom at the ankle. Both the flexion–extension and abduction–adduction degrees of freedom at the hip are actuated, as is one flexion–extension degree of freedom at the knee, and the ankle plantar–dorsi flexion (in the sagittal plane). The other three degrees of freedom (i.e., rotation and abduction–adduction at the ankle and rotation at the hip) are equipped with passive impedances using steel springs and elastomers. In total, each BLEEX leg has four powered degrees of freedom: hip joint, knee joint and ankle joint in sagittal plane and a hip abduction–adduction joint. In comparison with the movements in the sagittal plane, the actuators for hip abduction–adduction do not contribute to system control during level ground walking.

4. Design by Biological Analogy

4.1. Clinical Gait Analysis (CGA) Data

Since we intended to design an anthropomorphic exoskeleton with similar limb masses and inertias to a human, the required joint torques and power for the exoskeleton to perform a given motion were approximated to that required by a similarly sized human performing the same motion. Additionally, since the primary goal of a lower-extremity exoskeleton is locomotion, the joint torque and power requirements for the BLEEX were thus determined by analyzing the walking cycle shown in Fig. 2.

Human joint angles and torques for a typical walking cycle were obtained in the form of independently collected Clinical Gait Analysis (CGA) data. CGA angle data is typically collected via human video motion capture. CGA torque data is calculated by estimating limb masses and inertias and applying dynamic equations to the motion data. Given the variations in individual gait and measuring methods, three independent sources of CGA data (Kirtley; Winter; Linsell) were utilized for the analysis and design of BLEEX. This data was modified to yield estimates of exoskeleton actuation requirements. The modifications included: (1) scaling the joint torques to a 75 kg person (the projected weight of BLEEX and its payload not including its pilot); (2) scaling the data to represent the walking speed of one cycle per second (or about 1.3 m/s); and (3) adding the pelvic tilt angle (or lower back angle depending on data available) to the hip angle to yield a single hip angle between the torso and the thigh as shown in Fig. 3. This accounts for the reduced degrees of freedom of the exoskeleton. The following sections describe the use of CGA data and its implication for the exoskeleton design. The sign conventions used are shown in Fig. 3.

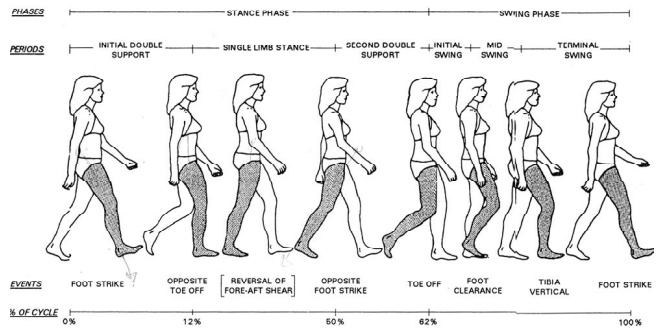


Fig. 2. The cycle begins with the start of stance phase (heel-strike) followed by toe-off and swing phase beginning at ~60% of the cycle (Rose and Gamble 1994).

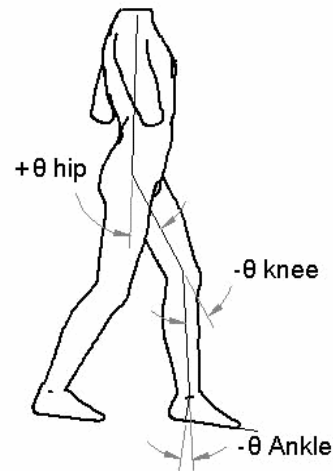


Fig. 3. Each joint angle is measured as the positive counterclockwise displacement of the distal link from the proximal link (zero in standing position) with the person oriented as shown. In the position shown, the hip angle is positive whereas both the knee and ankle angles are negative. Torque is measured as positive acting counterclockwise on the distal link.

4.2. The Ankle

Figure 4 shows the CGA ankle angle data for a 75 kg human walking on flat ground at approximately 1.3 m/s versus time. Although Fig. 4 shows a small range of motion while walking (approximately -20° to $+15^\circ$), greater ranges of motion are required for other movements. An average person can flex their ankles anywhere from -38° to $+35^\circ$ (Woodson et al. 1992). The BLEEX ankle was chosen to have a maximum flexibility of $\pm 45^\circ$ to compensate for the lack of several smaller degrees of freedom in the exoskeleton foot.

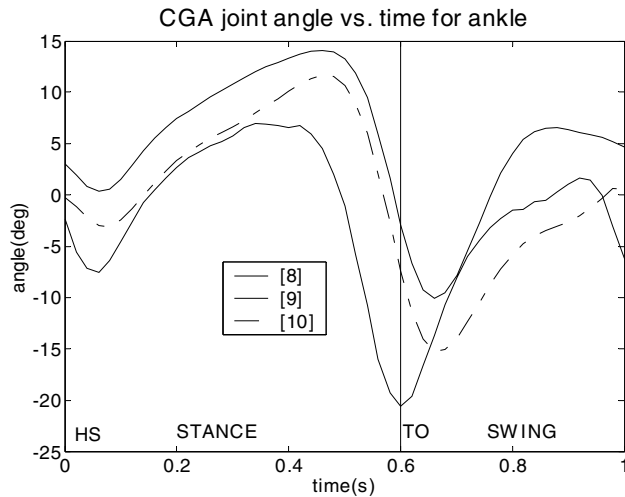


Fig. 4. Adjusted CGA data of the ankle flexion/extension angle. The minimum angle (extension) is around -20° and occurs just after toe-off. The maximum angle (flexion) is about $+15^\circ$ and occurs in the late stance phase. Through all gait analysis plots, TO denotes “Toe-Off” and HS denotes “Heel-Strike”. Throughout these figures, the numbers in square brackets refer to the references: [8] Kirtley; [9] Winter; [10] Linszell.

Figure 5 shows the adjusted CGA data of the ankle flexion/extension torque. The ankle torque is almost entirely negative—making unidirectional actuators an ideal actuation choice. This asymmetry also implies a preferred mounting orientation for asymmetric actuators (one-sided hydraulic cylinders). Conversely, if symmetric bi-directional actuators are considered, spring-loading would allow the use of low torque producing actuators. Although the ankle torque is large during stance, it is negligible during swing. This suggests a system that disengages the ankle actuators from the exoskeleton during swing to save power.

The instantaneous ankle mechanical power (shown in Fig. 6) is calculated by multiplying the joint angular velocity (derived from Fig. 4) and the instantaneous joint torque (Fig. 5). The ankle absorbs energy during the first half of the stance phase and releases energy just before toe off. The average ankle power is positive, indicating that power production is required at the ankle.

4.3. The Knee

The knee angle in Fig. 7 is characterized by knee flexion to create a horizontal hip trajectory. The knee buckles momentarily in early stance to absorb the impact of heel strike then undergoes a large flexion during swing. This knee flexion decreases the effective leg length, allowing the foot to clear the ground

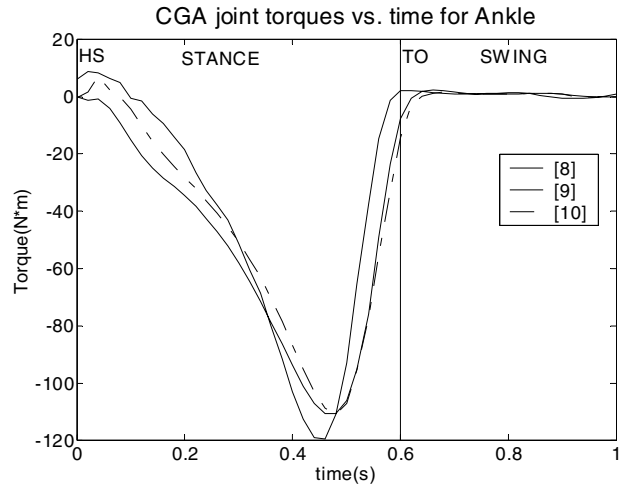


Fig. 5. Adjusted CGA data of the ankle flexion/extension torque. Peak negative torque (extension of the foot) is very large (-120 N m) and occurs in the late stance phase. The ankle torque during swing is quite small.

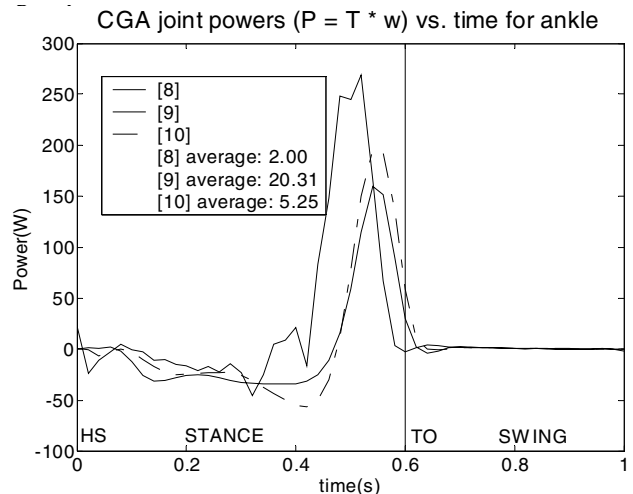


Fig. 6. Adjusted CGA data of the ankle flexion/extension instantaneous mechanical power. The average ankle power is positive, indicating the ankle does positive work and requires actuation.

when swinging forward. Although the walking knee flexion is limited to approximately 70° , the human has significantly more flexibility (up to 159° flexion possible when kneeling) (Woodson et al. 1992). The BLEEX knee flexion range was chosen to be 5° to 126° . The CGA based knee actuation torque is shown in Fig. 8.

The required knee torque has both positive and negative components, indicating the need for a bi-directional

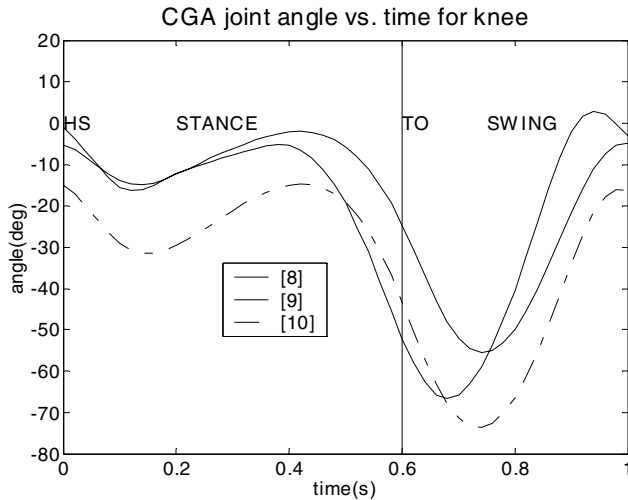


Fig. 7. Adjusted CGA data of the knee flexion/extension angle. The maximum knee angle is $\sim 0^\circ$ (any more would correspond to hyperextension of the knee) whereas the minimum angle is around -60° flexion, occurring in the early-mid swing phase, enabling the foot to clear the ground.

actuator. The highest peak torque is extension in early stance (~ 60 N m); hence asymmetric actuators should be biased to provide greater extension torque. Figure 9 shows the instantaneous mechanical power at the knee, which has both positive and negative components corresponding to power creation and absorption. The average power is negative and therefore the knee (on average) absorbs energy.

4.4 The Hip

Figure 10 details the hip angle while walking. The thigh moves in a sinusoidal pattern with the thigh flexed upward at heel-strike to allow foot-ground contact in front of the person. This is followed by an extension of the hip through most of stance phase and a flexion through the swing. The BLEEX hip angle is designed to have 10° extension and 115° flexion. The hip torque in Fig. 11 is relatively symmetric (-80 to $+60$ N m); hence a bi-directional hip actuator is required. Negative extension torque is required in early stance as the hip supports the load on the stance leg. Hip torque is positive in late stance and early swing as the hip propels the leg forward during swing. In late swing, the torque goes negative as the hip decelerates the leg prior to heel-strike. Figure 12 shows the instantaneous hip mechanical power. The hip absorbs energy during stance phase and injects it during toe-off to propel the torso forward.

4.5. Total CGA Power

The total CGA power shown in Fig. 13 was found by summing the absolute values of the instantaneous CGA powers

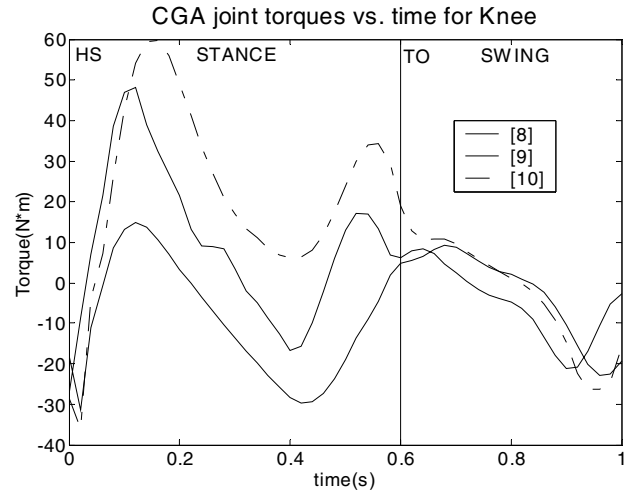


Fig. 8. Adjusted CGA data of the knee flexion/extension torque. An initial -35 N m flexion torque is required at heel strike, followed by large extension torques (~ 60 N m) to keep the knee from buckling in the stance phase.

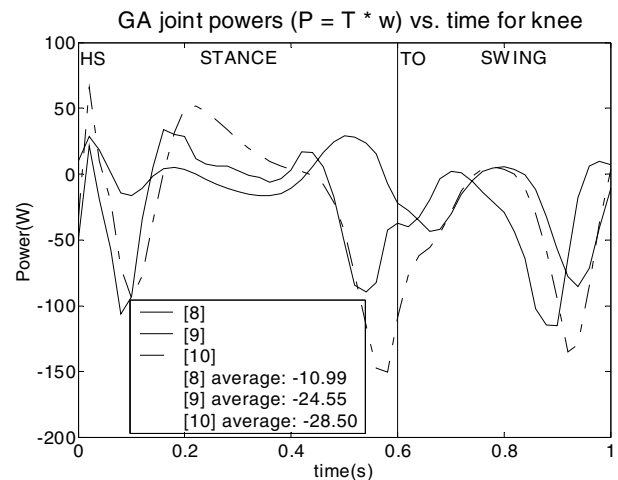


Fig. 9. Adjusted CGA data of the knee flexion/extension instantaneous mechanical power. The negative average indicates power dissipation.

for each joint (Figs. 6, 9, and 12) over both legs. The data in Fig. 13 shows that an average of 127 W to 210 W of mechanical power (i.e., torque \times speed) is required to move a 75 kg exoskeleton. This is independent of the type of power source. The absolute value of the joint powers in Figs. 6, 9, and 12 was used as a conservative measure (we assumed negative mechanical power in the exoskeleton does not indicate power regeneration). Since the opposite leg is phase shifted by half a cycle, the total CGA power in Fig. 13 has two peaks.

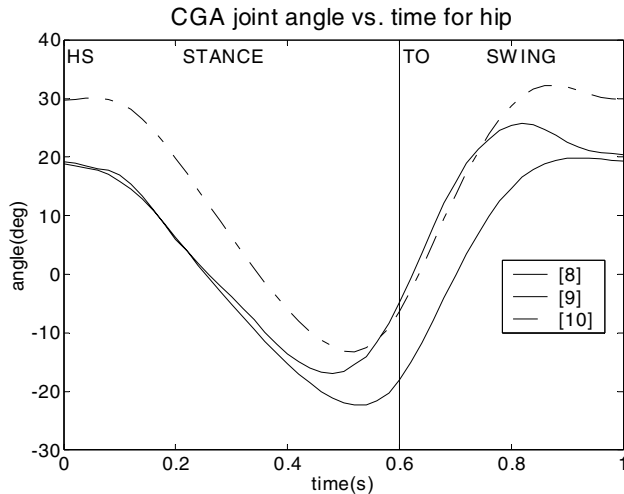


Fig. 10. Adjusted CGA data of the hip flexion/extension angle. The hip has an approximately sinusoidal behavior, with the thigh oscillating between being flexed upward $\approx +30^\circ$ to being extended back $\approx -20^\circ$.

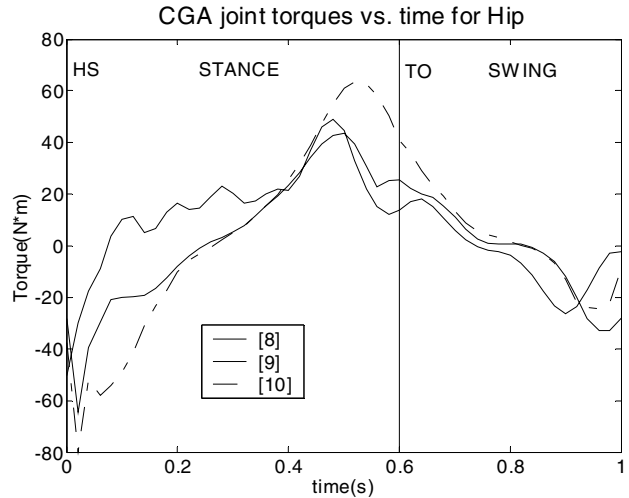


Fig. 11. Adjusted CGA data of the hip flexion/extension torque. The hip torque is bi-directional (≈ -80 N m extension to $\approx +60$ N m flexion).

4.6. BLEEX Range of Motion

At the very least, the BLEEX joint range of motion should be equal to the human range of motion during walking (shown in column 1 in Table 1), which can be found by examining Clinical Gait Analysis (CGA) data (Kirtley; Winter; Linskill). Safety dictates that the BLEEX range of motion should not be more than the operator's range of motion (shown in Column 3 of Table 1) (Woodson et al. 1992). For each degree of freedom, the second column of Table 1 lists the BLEEX range of motion, which is, in general, larger than the human range of motion during walking and less than the maximum range of human motion.

The exoskeleton should ideally have ranges of motion slightly less than the human's maximum range of motion. However, BLEEX uses linear actuators, so some of the joint ranges of motion are reduced to prevent the actuators' axes of motion from passing through the joint center. If this had not been prevented, the joint could reach a configuration where the actuator would be unable to produce a torque about its joint. Additionally, all the joint ranges of motion were tested and revised using plastic mockups. Several mock-ups (one is shown in Fig. 14) were designed and constructed not only for ergonomic evaluation but also for measurement of required range of motion. The experiments with the plastic mockups forced us to relocate and modify the range of motion for some of the degrees of freedom. For example, mock-up testing determined that the BLEEX ankle flexion/extension range of motion needs to be greater than the human ankle range of motion to accommodate the human foot's smaller degrees of freedom not modeled in the BLEEX foot.

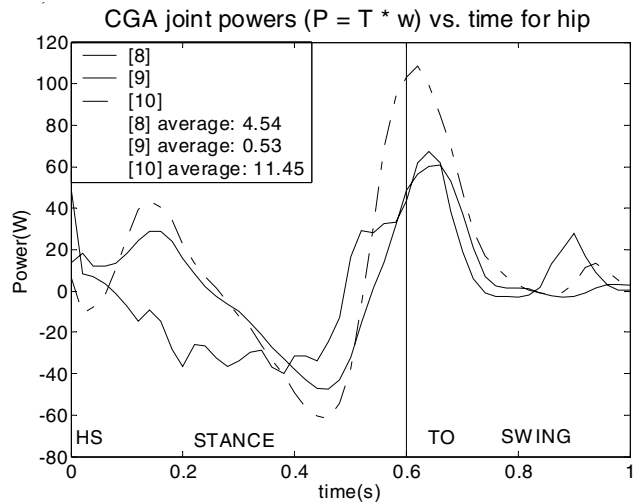


Fig. 12. Adjusted CGA data of the hip flexion/extension instantaneous mechanical power.

4.7. Actuation Selection and Modeling

Bi-directional lightweight linear hydraulic actuators were chosen to actuate the BLEEX degrees of freedom (Fig. 15) to ensure other maneuvers in addition to simple walking are allowed. The magnitudes of the maximum pushing and pulling forces ($F_{maxpush}$ and $F_{maxpull}$) that can be applied by a bi-directional actuator are given by (1) and (2) as a function of supply pressure (P_{supply}), actuator bore diameter ($actD$),

Table 1. BLEEX Joint Ranges of Motion

	Human Walking Maximum	BLEEX Maximum	Average Human Maximum
Ankle Flexion	14.1°	45°	35°
Ankle Extension	20.6°	45°	38°
Ankle Abduction	not available	20°	23°
Ankle Adduction	not available	20°	24°
Knee Flexion	73.5°	121°	159°
Hip Flexion	32.2°	121°	125°
Hip Extension	22.5°	10°	Not available
Hip Abduction	7.9°	16°	53°
Hip Adduction	6.4°	16°	31°
Total Rotation External	13.2°	35°	73°
Total Rotation Internal	1.6°	35°	66°

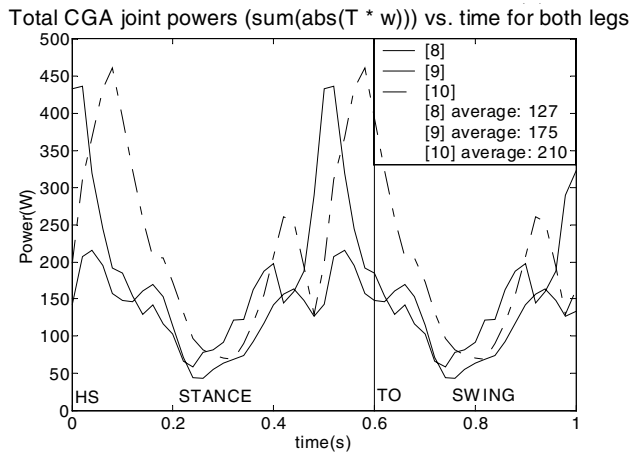


Fig. 13. Total required mechanical power of a 75 kg human walking over flat ground at approximately 1.3 m/s. This was calculated by summing the absolute values of the mechanical powers for the ankles, knees and hips.

and rod diameter ($rodD$).

$$F_{max\ push} = P_{supply} \cdot \frac{\pi (actD)^2}{4} \quad (1)$$

$$F_{max\ pull} = P_{supply} \cdot \frac{\pi (actD^2 - rodD^2)}{4} \quad (2)$$

Figure 16 shows a linear hydraulic actuator arranged to produce a joint torque. Vector expressions for the maximum possible torque from an extending and a contracting actuator (T_{push} and T_{pull}) are given by:

$$\vec{T}_{push} = F_{max\ push} \vec{R} \times \frac{\vec{C}}{|C|} \quad (3)$$

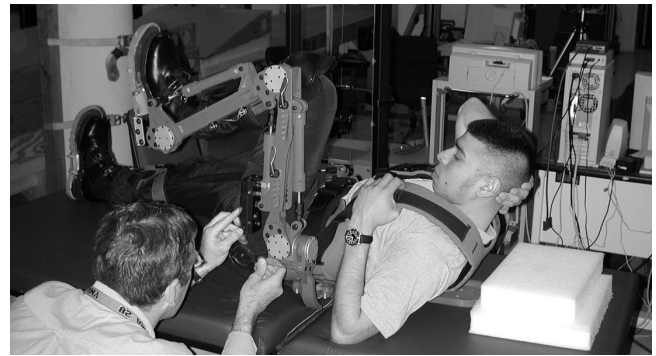


Fig. 14. One of the functional mock-ups of the exoskeleton architecture created at UC Berkeley to determine necessary degrees of freedom, ranges of motion, and ergonomic attachments. These prototypes were made by a Fused Deposition Modeling (FDM) machine.

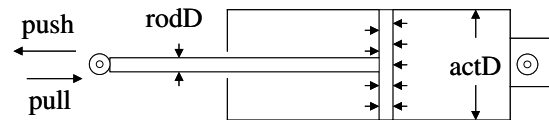


Fig. 15. Bi-directional linear hydraulic actuator schematic. Note that the area on which the internal pressure can act is different on the piston and rod sides of the actuator. This means that the actuator can push with more force than it can pull given the same supply pressure.

$$\vec{T}_{pull} = F_{max\ pull} \vec{R} \times \frac{\vec{C}}{|C|} \quad (4)$$

\vec{C} is a vector whose magnitude is the length of the actuator.

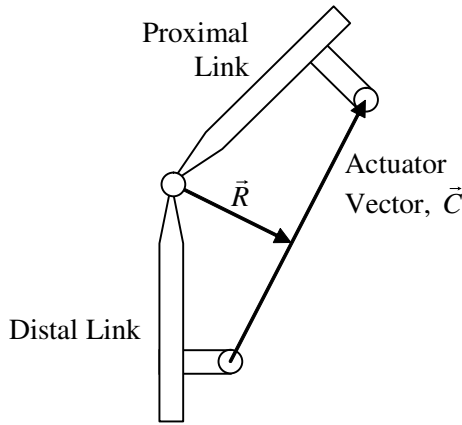


Fig. 16. Triangular configuration of a linear hydraulic actuator.

Figure 16 and equations (3) and (4) show that the placements of the actuator end points have a direct effect on the magnitude of the joint actuator torque. The farther the actuator is from the joint, the larger the actuator torque and volumetric displacements for a given angular joint motion. Similarly, actuators with larger cross-sections may produce more force and torque, but will require larger volumetric displacements for a given angular motion. Larger volumetric displacements correspond to higher hydraulic flows and increased power consumption for a given angular motion. The problem of actuation design is to find an actuator (i.e., cross-section area, minimum length, and stroke), location of the actuator end-points on two neighboring links, and a constant supply pressure such that the generated torque for each joint is slightly larger than is shown by Fig. 5, Fig. 8 and Fig. 11 over the entire range of motion (Fig. 4, Fig. 7 and Fig. 10), and subject to several constraints. These constraints include: (1) the actuators are available in discrete sizes (cross-section, minimum length, and stroke); (2) the minimum angular range of motion for each joint described in Section 4.6 needs to be guaranteed; (3) the actuator line of action must not pass through the joint; and (4) no interference between the actuators and the links should take place. In general, there is no unique solution, and there are a large number of feasible possibilities. An initial actuator size (cross-section, minimum length, and stroke), and one of the end-point positions were chosen for each joint. Combined with the required minimum angular range of motion (given in section 4.6), this determined the second actuator mount point (see graphical synthesis for the ankle in Fig. 17). The available actuator torque from (3) and (4) was then compared with the required torques in Fig. 5, Fig. 8 and Fig. 11. This process was iterated with different actuator sizes and mounting points until a solution was found.

Figures 18, 19 and 20 show the torque versus angle plots of the resulting BLEEX joints compared to human CGA data for the ankle, knee and hip. The actuator limit lines show both

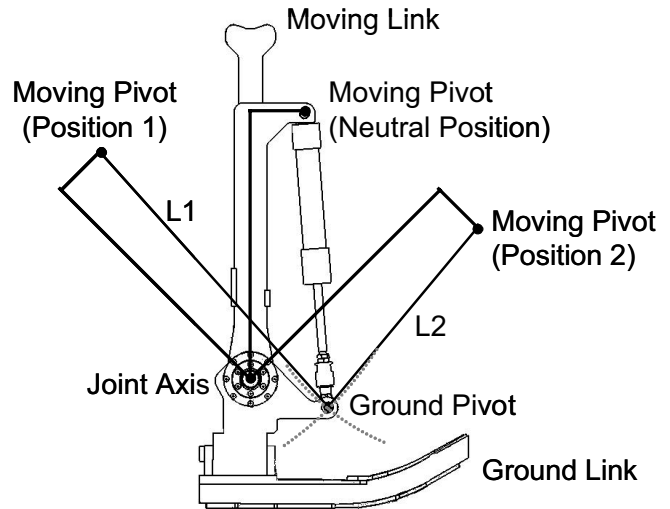


Fig. 17. Two-position kinematical synthesis of ankle actuator placement. A linear actuator of contracted length L2 and extended length L1 was chosen. The position of the moving pivot in the neutral position was chosen. This defined the moving pivot location at the limits of motion (positions 1 and 2). The position of the ground pivot was found by intersecting arcs of radii L1 and L2 centered at the moving pivot positions 1 and 2.

the available actuator torque and the range of motion of the joint. Figure 21 shows the physical manifestation of the linear actuator designs evaluated in Fig. 18, Fig. 19 and Fig. 20. The ankle requires predominately negative torque (Fig. 5); hence the ankle actuator is positioned anterior to the joint whereby its greater extension force capacity can be exploited. Similarly, the knee actuator is placed behind the knee, where it can apply greater required extension torques (Fig. 8).

4.8. BLEEX Hydraulic Flow and Power Consumption

The total required hydraulic flow shown in Fig. 22 is the sum of the hydraulic flows to each actuator. Individual actuator flows were found by multiplying the magnitude of the actuator linear velocity by the effective area of the actuator over a walking cycle, as shown in (5) and (6). Due to asymmetry, the flow while extending ($Q_{extension}$) differed from that while contracting ($Q_{contraction}$).

$$Q_{extension} \approx ABS \left[\left(\frac{\partial}{\partial t} |\vec{C}| \right) \cdot \frac{\pi (actD)^2}{4} \right] \quad (5)$$

$$Q_{contraction} \approx ABS \left[\left(\frac{\partial}{\partial t} |\vec{C}| \right) \cdot \frac{\pi ((actD)^2 - (rodD)^2)}{4} \right] \quad (6)$$

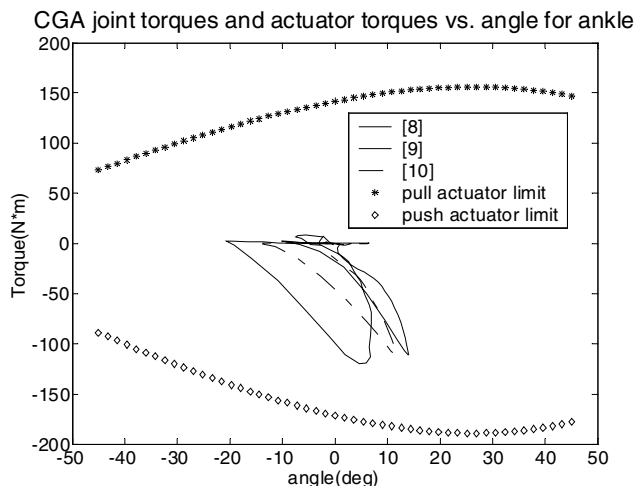


Fig. 18. Ankle torque versus angle. The actuator torque limits at 1000 psi exceed the adjusted CGA torque of Fig. 5 over the entire range of motion.

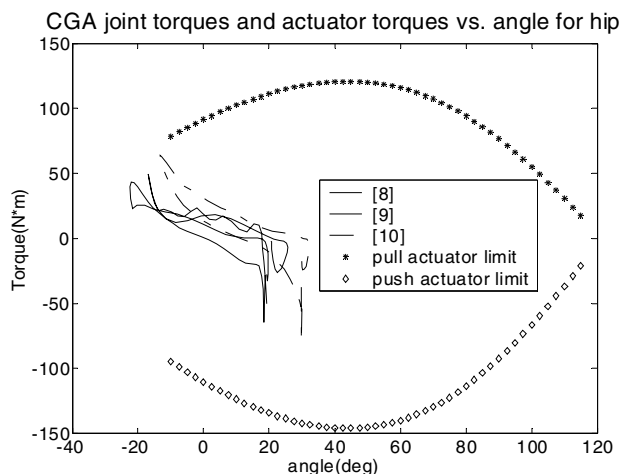


Fig. 20. Hip torque versus angle. The actuator torque limits at 1000 psi exceed the adjusted CGA torque of Fig. 11 over the entire range of motion.

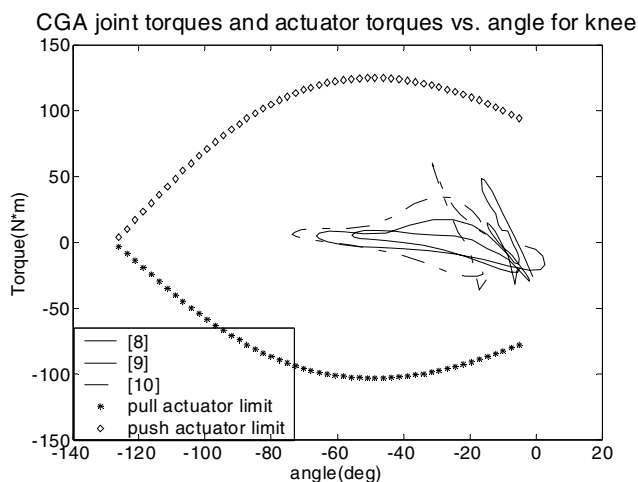


Fig. 19. Knee torque versus angle. The actuator torque limits at 1000 psi exceed the adjusted CGA torque of Fig. 8 over the entire range of motion.

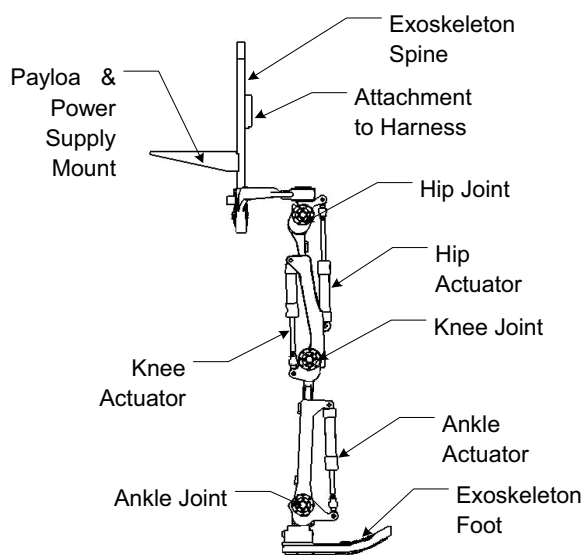


Fig. 21. Model of first-generation BLEEX prototype. This model shows the locations and orientations of the linear hydraulic actuators that support the weight of the exoskeleton and payload.

The total hydraulic power consumption of BLEEX was estimated by multiplying the supply pressure (1000 psi) by the total required hydraulic flow as shown in Fig. 23, which predicts a required 1.1–1.3 kW of hydraulic power (pressure \times flow) for the BLEEX to walk. This is anywhere from 5 to 7 times the average total mechanical power (torque \times speed) shown in Fig. 13. The information shown in Fig. 13 represents the mechanical power needed for a 75 kg person (or 75 kg exoskeleton) to walk according to the CGA data, while the data of Fig. 23 represents the hydraulic power for such exoskele-

ton. The difference between them is the losses due to pressure modulation in the servo-valves. In calculation of the hydraulic power, we considered a constant pressure (1000 psi); however, this constant pressure is reduced in the servo-valve to produce the proper amount of pressure for the actuators. The difference between hydraulic power consumed and mechanical power produced is wasted across the servo-valves. A hydraulic actuator operating at a fraction of its maximum torque capacity

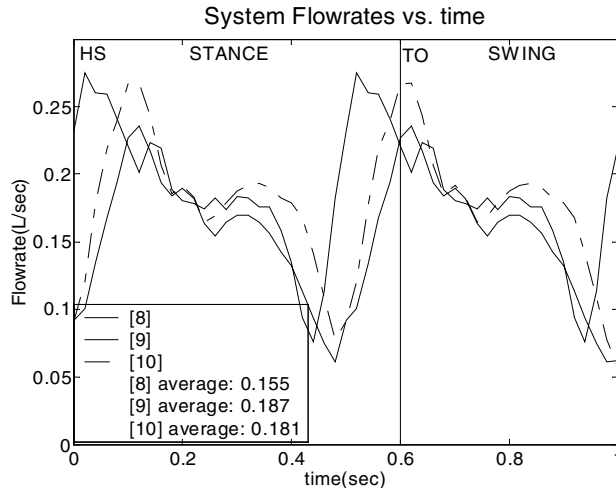


Fig. 22. BLEEX computed instantaneous total required hydraulic flow based on CGA data. Note that this data does not account for leakages.

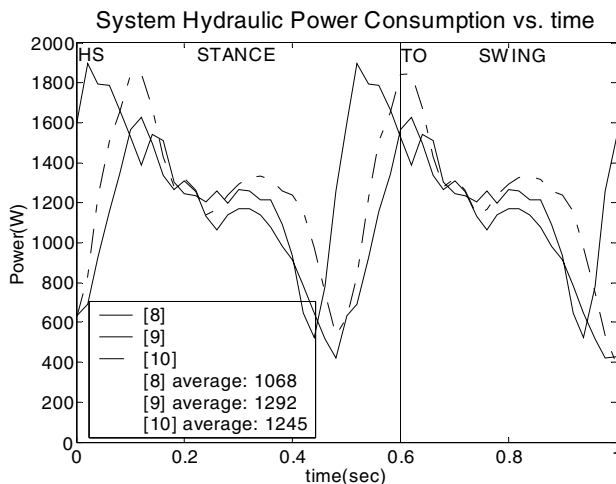


Fig. 23. BLEEX computed total hydraulic power consumption based on human CGA data.

consumes the same hydraulic power as if producing its full torque capacity over the same trajectory.

Although Fig. 23 shows that the BLEEX actuators require nominally 1.1–1.3 kW of hydraulic power to walk, more power is required for a successful implementation. The driving second-stage of each of the eight servovalves required an additional approximately 28 W, leading to a total of 240 W of additional hydraulic power consumption. Further analysis also indicated an additional 540 W of hydraulic power was required for some activities other than walking (i.e., climbing

stairs or ramps) and hip abduction actuators in non-sagittal plane. An estimated 200 W of electrical power was also required by the BLEEX control, sensors, servo-valves, and all electrical subsystems. The net power requirements of the BLEEX after addition of a 10% safety factor were determined to be ~ 2.27 kW (3 HP) of hydraulic power and 220 W of electrical power. This means 5.2 gpm (20 LPM) of hydraulic flow at 1000 psi (6.9 MPa). A small novel portable power source was designed to produce the required hydraulic and electric power for BLEEX [in print]. Hydraulic actuation and power supply requirements gleaned from the analysis above were used to design the prototype shown in Fig. 24. The linear hydraulic actuation sizes and placements evaluated in Figs. 18–21 were implemented. The hydraulic fluid flow rate estimates (5) and (6) were used to size both the servo-valves and the hydraulic lines of the system.

5. Exoskeleton Control

The control scheme needs no direct measurements from the pilot or the human-machine interface (e.g., no force sensors between the two); instead, the controller estimates, based on measurements from the exoskeleton only, how to move so that the wearer feels very little force. This control scheme is an effective method of generating locomotion when the contact location between the pilot and the exoskeleton is unknown and unpredictable (i.e., the exoskeleton and the pilot are in contact in a variety of places). This control method differs from compliance control methods employed for upper extremity exoskeletons (Kazerooni 1996; Kazerooni and Guo 1993), and haptic systems (Kazerooni and Her 1994; Kazerooni and Snyder 1995) because it requires no force sensor between the wearer and the exoskeleton.

The goal was to develop a control system for BLEEX with “high sensitivity” to external forces and torques. We were faced with two realistic concerns; the first was that an exoskeleton with high sensitivity to external forces and torques would respond to other external forces not initiated by its wearer. For example, if someone pushed against an exoskeleton that had high sensitivity to forces and torques, the exoskeleton would move in just the way it would move in response to the forces from its wearer. Although the fact that it does not stabilize its behavior on its own in response to other forces may sound like a serious problem, if it did (e.g., using a gyro), the pilot would receive motion from the exoskeleton unexpectedly and would have to struggle with it to avoid unwanted movement. The key to stabilizing the exoskeleton and preventing it from falling in response to external forces depends on the wearer’s ability to move quickly (e.g., step back or sideways) to create a stable situation for himself and the exoskeleton. For this, a very wide control bandwidth is needed so the exoskeleton can respond to both pilot’s voluntary and involuntary movements (i.e., reflexes).



Fig. 24. One of the Berkeley Lower Extremity Exoskeleton Prototypes. The limbs are enclosed by plastic covers (<http://bleex.me.berkeley.edu/bleex.htm>).

The pilot and BLEEX have rigid mechanical connections at the torso and the feet; everywhere else, the pilot and BLEEX have compliant or periodic contact. The connection at the torso is made using a vest shown in Fig. 24. One of the essential objectives in the design of the custom vest was to allow the distribution of the forces between BLEEX and the pilot, thereby preventing abrasion. The adjustment mechanisms in the vests allow for a snug fit to the pilot. The vests include rigid plates (with hole patterns) on their backs for connection to the BLEEX torso.

The pilot's shoes or boots (Fig. 25(a)) attach to the BLEEX feet using a modified quick-release binding mechanism similar to snowboard bindings (Fig. 25(b)). A plate with the quick-release mechanism is attached to the rigid heel section of the BLEEX foot. Early versions of the BLEEX system had the pilot wearing a standard boot that had a mating binding cleat secured to the heel. The cleat on the modified pilot boot does not interfere with normal wear when the pilot is unclipped from BLEEX. The BLEEX foot is composed of the rigid heel section with the binding mechanism and a compliant, but load bearing, toe section that begins at midfoot and extends to the toe. The BLEEX foot has a compressible rubber sole with a tread pattern that provides both shock-absorption and traction while walking. The rubber sole of the BLEEX foot contains embedded sensors, as shown in Fig. 27, that detect the trajectory of the BLEEX-ground reaction force starting from "heel-strike" to "toe-off." This information is used in the BLEEX controller to identify the BLEEX foot configuration relative to the ground.

Although biomechanical studies of walking frequently identify seven or more distinct phases of the human walking gait cycle, for simplicity in control we consider BLEEX to have three distinct phases (shown in Fig. 26) which lead to three different dynamic models:

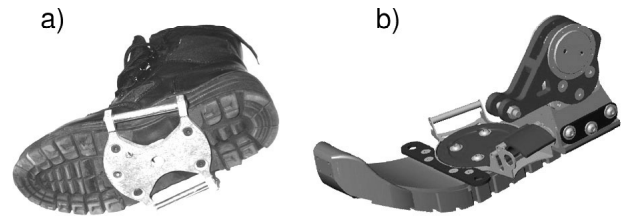


Fig. 25. Rigid attachment between (a) the pilot boot and (b) the BLEEX foot.

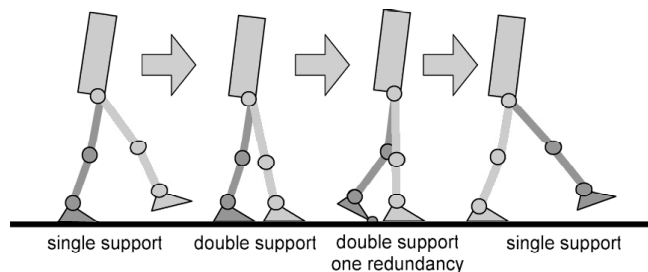


Fig. 26 Three phases of the BLEEX walking cycle.

Single support: one leg is in the stance configuration while another leg is in swing.

Double support: both legs are in stance configuration and situated flat on the ground.

Double support with one redundancy: both legs are in stance configuration, but one leg is situated flat on the ground while the other one is not.

Using the information from the sensors in the foot sole, the controller determines in which phase BLEEX is operating and which of the three dynamic models apply.

In our initial control design process, we decoupled the control of the abduction-adduction DOF at the hip from the control of joints in the sagittal plane. This is valid because we noticed through measurements that the abduction-adduction movements during normal walking (less than 0.9 m/s or 2 mph) are rather slow. In comparison with the movements in the sagittal plane, the abduction-adduction movements can be considered quasi-static maneuvers with little dynamical effects on the rest of system. This indicates that the exoskeleton dynamics in the sagittal plane are affected only by the abduction-adduction angle and not by the abduction-adduction dynamics. For the sake of brevity, the following sections describe the control method in the sagittal plane for a given set of abduction-adduction angles.

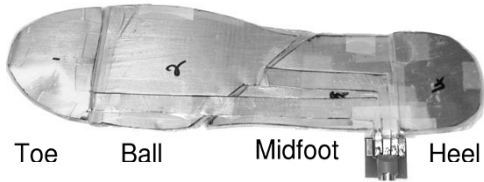


Fig. 27. The sensory system in one prototype BLEEX foot sole is composed of pressure sensitive semi-conductive rubber embedded in a polyurethane sole (Fig. 25(b)). This foot measures the ground reaction force profile at four locations: toe, ball, midfoot, and heel. This sensors measure the force between the exoskeleton and the ground; they do not measure the force between the exoskeleton and the person.

5.1. Single Support

In the single support phase, BLEEX is modeled as the 7-DOF serial link mechanism in the sagittal plane shown in Section 5.2. The dynamics of BLEEX can be written in the general form as:

$$M(\theta)\ddot{\theta} + C(\theta, \dot{\theta})\dot{\theta} + P(\theta) = T + d \quad (7)$$

where $\theta = [\theta_1 \ \theta_2 \ \dots \ \theta_7]^T$ and $T = [0 \ T_1 \ T_2 \ \dots \ T_6]^T$. M is a 7×7 inertia matrix and is a function of θ , $C(\theta, \dot{\theta})$ is a 7×7 centripetal and Coriolis matrix and is a function of θ and $\dot{\theta}$, and P is a 7×1 vector of gravitational torques and is a function of θ only. T is the 7×1 actuator torque vector with its first element set to zero since there is no actuator associated with joint angle θ_1 (i.e., angle between the BLEEX foot and the ground). d is the effective 7×1 torque vector imposed by the pilot on BLEEX at various locations. We choose the controller to be the inverse of the BLEEX dynamics scaled by, where α is an amplification number.

$$T = \hat{P}(\theta) + (1 - \alpha^{-1}) [\hat{M}(\theta)\ddot{\theta} + \hat{C}(\theta, \dot{\theta})\dot{\theta}] \quad (8)$$

$\hat{C}(\theta, \dot{\theta})$, $\hat{P}(\theta)$ and $\hat{M}(\theta)$ are estimates of the Coriolis matrix, gravity vector, and inertia matrix respectively for the system shown in Fig. 29. Note that equation (8) results in a 7×1 actuator torque. Since there is no actuator between the BLEEX foot and the ground, the torque prescribed by the first element of T must be provided by the pilot. Substituting T from equation (8) into equation (7) yields,

$$M(\theta)\ddot{\theta} + C(\theta, \dot{\theta})\dot{\theta} + P(\theta) = \hat{P}(\theta) + (1 - \alpha^{-1}) [\hat{M}(\theta)\ddot{\theta} + \hat{C}(\theta, \dot{\theta})\dot{\theta}] + d \quad (9)$$

In the limit when $M(\theta) = \hat{M}(\theta)$, $C(\theta, \dot{\theta}) = \hat{C}(\theta, \dot{\theta})$, $P(\theta) = \hat{P}(\theta)$, and α is sufficiently large, d will approach zero, meaning the pilot can walk as if BLEEX did not exist. However, it can be seen from equation (9) that the force felt by the pilot is a function of α and the accuracy of the estimates

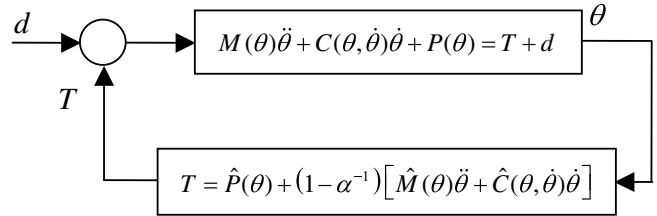


Fig. 28. The controller creates a loop gain slightly smaller than unity which results in an almost unstable system.

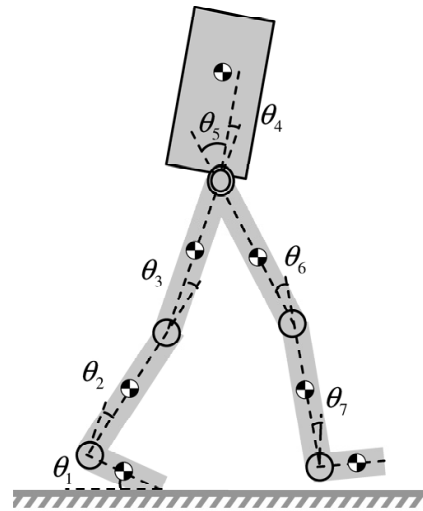


Fig. 29. Sagittal plane representation of BLEEX in the single stance phase. The “torso” includes the combined exoskeleton torso mechanism, payload, control computer, and power source.

$\hat{C}(\theta, \dot{\theta})$, $\hat{P}(\theta)$, and $\hat{M}(\theta)$. In general, the more accurately the system is modeled, the less the human force, d , will be. In the presence of variations in abduction–adduction angles, only $P(\theta)$ in equations (7) and (8) needs to be modified.

To get the above method working properly, one needs to understand the dynamics of the exoskeleton quite well, as the controller is heavily model based. One can see this problem as a tradeoff: the design approach described above requires no sensor (e.g., force or EMG) in the interface between the pilot and the exoskeleton; one can push and pull against the exoskeleton in any direction and at any location without measuring any variables on the interface. However, the control method requires a very good model of the system.

One can show through a simple single degree of freedom linear system that the control implemented here simply uses the inverse dynamics of the plant (the exoskeleton here) scaled by as a positive feedback controller (Kazerooni and Steger

2006). This reveals that the control scheme described here almost destabilizes the system since it leads to an overall loop gain slightly smaller than unity: $(1 - \alpha^{-1})$. This almost-unity gain loop not only leads to an almost unstable system but also results in a large sensitivity to all forces and torques. Fig. 28 schematically represents the closed loop control block diagram in a non-linear form. The forward loop represents the dynamics of the system and the feedback loop is an approximation of the inverse of the forward loop dynamics. Examination of the system of Fig. 28 shows that the loop gain is slightly smaller than unity (almost unstable system). This means this controller—which does not stabilize BLEEX – forces the exoskeleton to follow wide-bandwidth human maneuvers while carrying heavy loads. We have come to believe, to rephrase Friedrich Nietzsche, that that which does not stabilize, will only make us stronger.

5.2. Double Support

In the double support phase, both BLEEX feet are flat on the ground. The exoskeleton is modeled as two planar 3-DOF serial link mechanisms that are connected to each other along their uppermost link as shown in Fig. 30(a). The dynamics for these serial links are represented by equations (10) and (11).

$$M_L(m_{TL}, \theta_L) \ddot{\theta}_L + C_L(m_{TL}, \dot{\theta}_L, \theta_L) \dot{\theta}_L + P_L(m_{TL}, \theta_L) = T_L + d_L \quad (10)$$

$$M_R(m_{TR}, \theta_R) \ddot{\theta}_R + C_R(m_{TR}, \dot{\theta}_R, \theta_R) \dot{\theta}_R + P_R(m_{TR}, \theta_R) = T_R + d_R \quad (11)$$

where: $\theta_L = [\theta_{L1} \ \theta_{L2} \ \theta_{L3}]^T$ and $\theta_R = [\theta_{R1} \ \theta_{R2} \ \theta_{R3}]^T$. m_{TR} and m_{TL} are effective torso masses supported by each leg and m_T is the total torso mass such that:

$$m_T = m_{TR} + m_{TL} \quad (12)$$

The contributions of m_T on each leg (i.e., m_{TL} and m_{TR}) are chosen as functions of the location of the torso center of mass relative to the locations of the ankles such that

$$\frac{m_{TR}}{m_{TL}} = \frac{x_{TL}}{x_{TR}} \quad (13)$$

where x_{TL} is the horizontal distance between the torso center of mass and the left ankle, and x_{TR} is the horizontal distance between the torso center of mass and the right ankle. For example, if the center of mass of the torso is located directly above the right leg, then $m_{TL} = 0$ and $m_{TR} = m_T$. Similar to the single stance phase, the controllers are chosen such that

$$T_L = \hat{P}_L(m_{TL}, \theta_L) + (1 - \alpha^{-1}) \left[\hat{M}_L(m_{TL}, \theta_L) \ddot{\theta}_L + \hat{C}_L(m_{TL}, \theta_L, \dot{\theta}_L) \dot{\theta}_L \right] \quad (14)$$

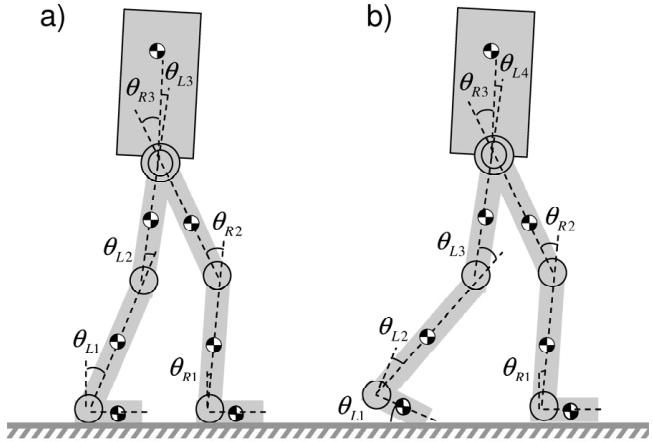


Fig. 30. Sagittal plane representation of BLEEX in (a) the double support phase and (b) the double support phase with one redundancy.

$$T_R = \hat{P}_R(m_{TR}, \theta_R) + (1 - \alpha^{-1}) \left[\hat{M}_R(m_{TR}, \theta_R) \ddot{\theta}_R + \hat{C}_R(m_{TR}, \theta_R, \dot{\theta}_R) \dot{\theta}_R \right] \quad (15)$$

Needless to say, (13) is valid only for quasi-static conditions, where the accelerations and velocities are small. This is in fact the case, since in the double support phase, both legs are on the ground and BLEEX's angular acceleration and velocities are quite small. This allows us to simplify equations (14) and (15) during slow walking by removing all terms except the estimates of the gravitational vectors.

5.3. Double Support with One Redundancy

Double support with one redundancy is modeled as a 3-DOF serial link mechanism for the stance leg with the foot flat on the ground and a 4-DOF serial link mechanism for the stance leg that is not completely on the ground (Fig. 30(b)). Each serial link supports a portion of the torso weight. The dynamics for these serial links are represented by equations (16) and (17), where, at the specific moment shown in Figure 29(b), the left leg has four degrees of freedom and the right leg has three degrees of freedom.

$$M_L(m_{TL}, \theta_L) \ddot{\theta}_L + C_L(m_{TL}, \dot{\theta}_L, \theta_L) \dot{\theta}_L + P_L(m_{TL}, \theta_L) = T_L + d_L \quad (16)$$

$$M_R(m_{TR}, \theta_R) \ddot{\theta}_R + C_R(m_{TR}, \dot{\theta}_R, \theta_R) \dot{\theta}_R + P_R(m_{TR}, \theta_R) = T_R + d_R \quad (17)$$

where

$$\theta_L = [\theta_{L1} \ \theta_{L2} \ \theta_{L3} \ \theta_{L4}]^T, \theta_R = [\theta_{R1} \ \theta_{R2} \ \theta_{R3}]^T$$

$$T_L = [0 \ T_{L1} \ T_{L2} \ T_{L3}]^T$$

and

$$T_R = [T_{R1} \quad T_{R2} \quad T_{R3}]^T$$

m_{TR} and m_{TL} are the effective torso masses supported by each leg and are computed similarly to the double support case, by use of (13). Utilizing (16) and (17) as dynamic models of the exoskeleton, (14) and (15) are used as controllers in this case. Clearly, the actuator torque vector associated with the leg that has four degrees of freedom (e.g., T_L in the case shown in Fig. 30(b)) is a 4×1 vector. As in the single support phase, the torque prescribed by the first element of T must be provided by the pilot because there is no actuator between the BLEEX foot and the ground. As BLEEX goes through the various phases shown in Fig. 26, the sensors shown in Section 5.1 detect which leg has four degrees of freedom and which leg has three degrees of freedom. The controller then chooses the appropriate algorithm for each leg.

The Berkeley Lower Extremity Exoskeleton (BLEEX) is not a typical servo-mechanism. While providing disturbance rejection along some axes preventing motion in response to gravitational forces, BLEEX actually encourages motion along other axes in response to pilot interface forces. This characteristic requires large sensitivity to pilot forces, which invalidates certain assumptions of the standard control design methodologies, and thus requires a new design approach. The controller described here uses the inverse dynamics of the exoskeleton as a positive feedback controller. Our current experiments with BLEEX have shown that this control scheme has two superior characteristics: (1) it allows for a wide bandwidth control system to follow all human voluntary and non-voluntary maneuvers during level walking at a speed of 1.3 m/s; (2) it is unaffected by changing human dynamics. The tradeoff is that it requires a relatively accurate model of the system. BLEEX is currently the strongest, successfully walking, untethered lower extremity exoskeleton in existence, and has been worn on a treadmill at speeds up to 1.3 m/s.

6. Conclusions

Human kinematics, dynamics and CGA data are used to design BLEEX. The BLEEX leg has seven degrees of freedom and four of them are actuated (flexion/extension at the ankle, knee, and hip and abduction/adduction at the hip). The actuator sizes, actuator mounting points, and servo valves were selected utilizing human CGA data. The hip abduction/adduction actuators do not contribute to motion in the sagittal plane. The controller uses the inverse dynamics of the system as a positive feedback, resulting in an almost unstable system and therefore it requires a relatively accurate model of the leg. This provides high sensitivity to all forces and torques and therefore encourages motion in response to pilot interface forces. The pilot can move the leg along all directions without the use of any force sensor between the pilot and the exoskeleton.

References

- Amundson, K., Raade, J., Harding, N., and Kazerooni, H. (2005). Hybrid hydraulic-electric power unit for field and service robots. *Proceedings of IEEE Intelligent Robots and Systems*, Edmonton, Canada, August.
- General Electric Co. (1969). Hardiman I arm test. General Electric Report S-70-1019, Schenectady, NY.
- General Electric Co. (1968). Hardiman I prototype project, special interim study. General Electric Report S-68-1060, Schenectady, NY.
- Granosik, G. and Borenstein, J. (2004). Minimizing air consumption of pneumatic actuators in mobile robots. *Proceedings of IEEE International Conference on Robotics and Automation*, New Orleans, LA., pp. 3643–3639.
- Groshaw, P. F. (1969). Hardiman I arm test, Hardiman I prototype. General Electric Report S-70-1019, Schenectady, NY.
- Hirai, K., Hirose, M., Haikawa, Y., and Takenaka, T. (1998). The development of Honda humanoid robot. *Proceedings of the 1998 IEEE International Conference on Robotics & Automation*, Leuven, Belgium.
- Hristic, D. and Vukobratovic, M. (1973). Development of active aids for handicapped. *Proceedings of the third International Conference on Bio-medical Engineering*, Sorrento, Italy.
- Kawamoto, H. and Sankai, Y. (2002). Power assist system HAL-3 for gait disorder person. ICCHP, Austria, July.
- Kawamoto, H., Kanbe, S., and Sankai, Y. (2003). Power assist method for HAL-3 estimating operator's intention based on motion information. *Proceedings of the 2003 IEEE Workshop on Robot and Human Interactive Communication*, Millbrae, CA, pp. 67–72.
- Kazerooni, H. (1990). Human-robot interaction via the transfer of power and information signals. *IEEE Transactions on Systems and Cybernetics*, **20**(2): 450–463.
- Kazerooni, H. (1996). The human power amplifier technology at the University of California, Berkeley. *Journal of Robotics and Autonomous Systems*, **19**: 179–187.
- Kazerooni, H. and Guo, J. (1993). Human extenders. *ASME Journal of Dynamic Systems, Measurements, and Control*, **115**(2B): 281–289.
- Kazerooni, H. and Her, M. (1994). The dynamics and control of a haptic interface device. *IEEE Transactions on Robotics and Automation*, **10**(4): 453–464.
- Kazerooni, H. and Snyder, T. (1995). A case study on dynamics of haptic devices: human induced instability in powered hand controllers. *AIAA Journal of Guidance, Control, and Dynamics*, **18**(1): 108–113.
- Kazerooni, H. and Steger, R. (2006). The Berkeley Lower Extremity Exoskeletons. *ASME Journal of Dynamics Systems, Measurements and Control*, **128**: 14–25.
- Kim, S., Anwar, G., and Kazerooni, H. (2004). High-speed communication network for controls with application on

- the exoskeleton. *American Control Conference*, Boston, June.
- Kim, S. and Kazerooni, H. (2004). High speed ring-based distributed networked control system for real-time multi-variable applications. ASME International Mechanical Engineering Congress, Anaheim, CA, November.
- Kirtley, C. CGA Normative Gait Database, Hong Kong Polytechnic University, 10 Young Adults. Available: <http://guardian.curtin.edu.au/cga/data/>
- Linskell, J. CGA Normative Gait Database, Limb Fitting Centre, Dundee, Scotland, Young Adult. Available: <http://guardian.curtin.edu.au/cga/data/>
- Makinson, B. J. (1971). Research and development prototype for machine augmentation of human strength and endurance, Hardiman I Project. General Electric Report S-71-1056, Schenectady, NY.
- Mizen, N. J. (1965). Preliminary design for the shoulders and arms of a powered, exoskeletal structure. Cornell Aeronautical Laboratory Report VO-1692-V-4.
- Mosher, R. S. (1960). Force-reflecting electrohydraulic manipulator. *Electro-Technology*, December, 139–148.
- Pratt, J., Krupp, B., Morse, C., and Collins, S. (2004). The RoboKnee: an exoskeleton for enhancing strength and endurance during walking. *IEEE Conference on Robotics and Automation*, New Orleans.
- Raade, J. and Kazerooni, H. (2004). Analysis and design of a novel power supply for mobile robots. *Proceedings of IEEE International Conference on Robotics and Automation*, New Orleans, LA, April.
- Raibert, M. (1986). Legged robots, in Legged robots that balance. *Communications of the ACM*, **29**(6): 250–258.
- Riener, R., Rabuffetti, M., and Frigo, C. (2002). Stair ascent and descent at different inclinations. *Gait and Posture*, **15**: 32–34.
- Rose, J. and Gamble, J. G. (1994). *Human Walking*, 2nd edn. Williams & Wilkins, Baltimore, p. 26.
- Vukobratovic, M., Ciric, V., and Hristic, D. (1972). Contribution to the study of active exoskeletons. *Proceedings of the 5th IFAC Congress*, Paris.
- Winter, A. International Society of Biomechanics, Biomechanical Data Resources, Gait Data. Available: <http://www.isbweb.org/data/>
- Woodson, W., Tillman, B., and Tillman, P. (1992). *Human Factors Design Handbook*. McGraw-Hill, New York, pp. 550–552.